Measuring vacuum component impedance for the Argonne Advanced Photon Source upgrade

Medani P. Sangroula*

Physics Department, Illinois Institute of Technology, Chicago, Illinois 60616 USA

Ryan R. Lindberg, Robert M. Lill, and Randall Zabel

Advanced Photon Source, Argonne National Laboratory, Argonne, Illinois 60439 USA

(Received 7 July 2020; accepted 27 July 2020; published 19 August 2020)

The Advanced Photon Source plans to upgrade to a multibend achromat (MBA) lattice that will dramatically decrease the electron beam emittance, thereby enhancing the x-ray brightness by two to three orders of magnitude. Electron beam focusing in the MBA requires small-aperture vacuum components that must also have a small impedance so as to minimize rf-heating and collective instabilities. As part of this effort, this paper focuses on coupling impedance measurements and analysis of certain critical Advanced Photon Source Upgrade vacuum components. Impedance measurements of accelerator components have traditionally been done with the coaxial wire method, which is based on the fact that the Transverse Electro-Magnetic (TEM) mode of the coaxial cable can mimic the Coulomb field of a particle beam; however this measurement technique has various limitations. This paper describes our approach to measure the coupling impedance using a Goubau line (G-line), which is essentially a single wire transmission line designed to propagate Sommerfeld-like surface waves whose fundamental Transverse Magnetic (TM) mode mimics the Coulomb field of a relativistic particle beam. We describe in detail the measurement procedure that we have developed for the G-line, including the measurement setup and proper definition of a reference, measurement procedure and advantages, and our experience regarding how to reduce systematic experimental error that we learned over the course of the measurements. Starting with our initial suite of measurements and simulations designed to benchmark and validate the novel G-line based measurement technique, we present the measured results for several Advanced Photon Source Upgrade vacuum components, including those of two rf-gasket designs and the beam position monitor-bellows assembly.

DOI: 10.1103/PhysRevAccelBeams.23.082803

I. INTRODUCTION

Ultralow emittance storage rings based on multibend achromat lattices can provide a generational leap in x-ray performance by increasing the brightness and coherent flux by two to three orders in magnitude [1–3]. The compact and strong magnets for such lattices demand small gap apertures, which in turn may lead to an increased interaction between the electron beam and the chamber walls. This strong interaction between the beam and the vacuum chamber can lead to various deleterious collective effects including an increase in energy spread, a degradation of beam quality or even beam loss, overheating of vacuum components, etc., [4]. The strength of this interaction is typically characterized by the coupling impedance that can be associated with each vacuum component.

Although the impedance is a well-established concept, predicting it in a real accelerator is somewhat challenging. For example, the recent work by Smaluk *et al.* [5] compared the simulated impedance budget with beam-based measurements for 15 storage rings, and reported a significant discrepancy between these two results. One possible explanation could be that the even the best impedance predictions using the most sophisticated codes are only as good as the underlying model of the component. Typically, the simulated structure represents an ideal design which may miss subtle changes made to ease its production, or fail to adequately account for manufacturing tolerances. To try and minimize these issues the Advanced Photon Source Upgrade (APS-U) project has chosen to assess the impedance of various components using a combination of sophisticated electromagnetic simulation and rf bench measurements. In this paper we describe our experimental efforts to measure the longitudinal impedance of a variety of APS-U vacuum components.

*msangroul@bnl.gov

The conventional coaxial wire method, in which the TEM mode of a coaxial wire simulates the Coulomb field of a relativistic beam, has a long established history of measuring impedance [6–10]. One major drawback of this technique is its need for a matching network of resistors whose frequency dependence limits the bandwidth of the measurement. If not accounted for, this can lead to higher noise and false signals at higher frequencies due to the appearance of higher order modes (HOMs). Some of the challenges associated with these HOMs can be reduced by, for example, using an appropriate combination of resistive matching outside and rf-absorbing foam inside the device under test (DUT) [11,12], but this is very challenging if the DUT is a closed system.

Another issue with the traditional method is that it typically requires a relatively large-diameter central conductor to obtain a suitable characteristic impedance of the DUT. The large inner conductor results in larger perturbations to the DUT, and furthermore leads to greater uncertainties in the position of the chamber axis [13]. While one can consider improving this situation by using a thin central conductor, the associated errors can be substantial [8], and the resulting large characteristic impedance will require a suitably designed matching network.

The recently developed Goubau line based test fixture [13–15] can overcome most of the issues that arise in the traditional method, especially at higher frequencies. The Goubau line [14–17] is a dielectric coated single wire transmission line in which the fundamental TM mode of the surface wave has an electric field that mimics the properties of the Coulomb field of a relativistic particle beam. Once an appropriate launching and receiving design (that we describe later) has been made, the G-line setup does not require any additional matching networks, and can be used with a wide range of DUTs with no change in design. While the G-line has been used as a transmission line for a long time, its application as a diagnostic device in the accelerator community began about a decade ago, and its application to impedance measurements began a few years ago [13,18]. In what follows we describe the design and use of this technique to evaluate the impedance of some critical APS-U vacuum components.

This paper is organized as follows. In Sec. II we describe the novel G-line method, starting with a brief mathematical description based on that found in Ref. [15,19], and proceeding to a detailed description of the experimental design and our measurement procedures. Section III describes how we benchmarked the G-line setup using a relatively simple and well-known pillbox-type cavity, and compares impedance results between measurement and simulation. Finally, we show in Sec. IV the measured results for APS-U vacuum chamber components including detailed results for two rf-gasket designs and the beam position monitor (BPM)-bellows assembly, along with a brief description of our measurements of a gate valve liner and pumping cross.

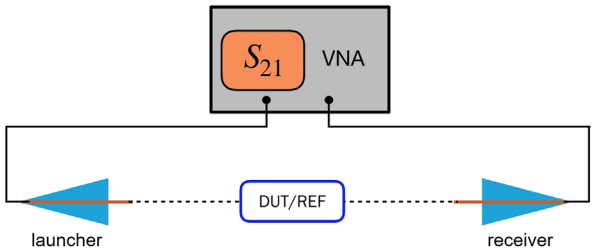

FIG. 1. Cartoon picture showing the schematic of the G-line setup.

II. GOUBAU-LINE (G-LINE)

The Goubau line [14,16,17] is a dielectric coated, single wire transmission line that transmits signals via surface waves. Early analysis of electromagnetic surface waves was done by Sommerfeld [20] and Zenneck [21], who showed that an electromagnetic wave could be supported at the cylindrical interface between a metallic wire and air. Although Sommerfeld waves have a theoretical attenuation much smaller than that in coaxial cables or rigid waveguides, their practical application is limited due to the fact that in low-loss systems the physical extent of the electromagnetic fields becomes very large [16,22].

Nonradiating surface waves of bounded extent can be supported by modifying the surface of the central conductor [23]; for example, a perfectly conducting wire that is coated with a dielectric material can support TM surface waves of low loss and small extent [23,24]. In 1950 George Goubau [16] showed how to employ these waves for signaling applications, and we call the resulting transmission line a Goubau line (G-line). Importantly, Goubau described tapered structures that can efficiently couple the quasi-TEM mode of a coaxial cable to the TM mode of the guided surface wave.

In the vicinity of the wire, the G-line's fundamental TM mode mimics the electromagnetic field of a relativistic electron beam. This led Ref. [14] to suggest that a G-line could be used by the accelerator community to experimentally test how a relativistic electron beam would interact with a variety of accelerator vacuum components. The Goubau line is superior to the traditional coaxial wire method in numerous respects: the G-line setup is simple since it does not require a complicated matching network; it perturbs the boundary conditions less due to the micron sized wire; it provides more accurate impedance matching; and it enables broad-band measurement [17,25]. A simple schematic cartoon picture of the G-line setup is shown in Fig. 1, where the blue cones facing each other represent a surface wave launcher and a receiver (also called horns), the dashed black line indicates the thin dielectric coated metallic wire which connects the launcher and receiver,

and each of these horns are connected to a vector network analyzer using two coaxial cables.

The G-line has been used by several groups to characterize beam position monitors (BPMs) and current transformers [15,17,19,26]. Simulations showing the G-line's potential to assess vacuum component impedance were described in Refs. [13,25], while the first experimental impedance measurements from a G-line were reported in Ref. [18]. The latter experimental setup differs from ours in that Ref. [18] replaced the receiver cone in Fig. 1 with rf-absorbers, and determined the impedance from the S_{11} reflection coefficient; typically, measurements based on the S_{11} is not as accurate as those that employ the S_{21} transmission coefficient [8].

A. Brief theory of G-line surface waves

The mathematical theory describing surface waves on a dielectric-coated wire can be found in many places (see, e.g., [15,16,19,22]). In this section we will review that part of the theory that is relevant to understanding the design of our experimental apparatus, paying particular attention to the extent to which the fields mimic a relativistic electron beam and fall off $\sim 1/r$, where r is the radial distance from beam axis. After a certain radial distance, the fields decay exponentially as illustrated in the Ref. [15].

We consider a metallic wire with radius a that is coated with a thin dielectric material of thickness $d = b - a$, so that the outer radius of the coated wire is b. We adopt cylindrical coordinates and assume periodic solutions in z. Inside the dielectric, the radial solution is given by a sum of the Bessel function $J_n(x)$ and the Neumann function $Y_n(x)$, so that for $a \le r \le b$ the electromagnetic fields are [16]

$$E_r = A\frac{l}{\gamma_d}[J_1(\gamma_d r) + mY_1(\gamma_d r)]e^{-i(\omega t - lz)} \tag{1a}$$

$$B_\phi = A\frac{k_d^2}{\omega\gamma_d}[J_1(\gamma_d r) + mY_1(\gamma_d r)]e^{-i(\omega t - lz)} \tag{1b}$$

$$E_z = iA[J_0(\gamma_d r) + mY_0(\gamma_d r)]e^{-i(\omega t - lz)}, \tag{1c}$$

where A is an amplitude factor and m is a function that will be determined by the boundary conditions. Equation (1) defines the solutions in terms of the frequency ω and propagation constant l, whose relation to other quantities is given by

$$\gamma_d^2 = k_d^2 - l^2 = \mu_d\epsilon_d\omega^2 - l^2 = \epsilon_r k_0^2 - l^2, \tag{2}$$

where the relative dielectric constant $\epsilon_r = \epsilon_d/\epsilon_0$, the dielectric permeability $\mu_d = \mu_0$ for a nonmagnetic material, and $k_0 = \omega/c$. In free space outside the wire we similarly define $\gamma_0^2 = k_0^2 - l^2$, which we see results in

$$\gamma_d^2 - \gamma_0^2 = k_d^2 - k_0^2 = k_0^2(\epsilon_r - 1). \tag{3}$$

The guided wave solutions are fully specified by enforcing the continuity of $\mu E_z/B_\phi$ at both interfaces. Inside the perfectly conducting wire we have $E_z = 0$, so that the boundary matching to (1c) at $r = a$ implies that $m = -J_0(\gamma_d a)/Y_0(\gamma_d a)$. Outside the wire the bounded, cylindrically symmetric solutions are given by the Hankel functions of first kind $H_0^{(1)}$ and $H_1^{(1)}$, and we have

$$\frac{E_z}{B_\phi/\mu} = \frac{\mu_0\omega\gamma_0}{k_0^2}\frac{H_0^{(1)}(\gamma_0 r)}{H_1^{(1)}(\gamma_0 r)} \quad \text{if } r \ge b. \tag{4}$$

Equating (4) at $r = b$ to the same ratio from (1) results in

$$\frac{\gamma_d}{\epsilon_r}\left[\frac{J_0(\gamma_d b)Y_0(\gamma_d a) - J_0(\gamma_d a)Y_0(\gamma_d b)}{J_1(\gamma_d b)Y_0(\gamma_d a) - J_0(\gamma_d a)Y_1(\gamma_d b)}\right] \approx -\frac{\gamma_d^2 b}{\epsilon_r}\ln\left(\frac{b}{a}\right) = \gamma_0\frac{H_0^{(1)}(\gamma_0 b)}{H_1^{(1)}(\gamma_0 b)}. \tag{5}$$

The second line employs a useful approximation to the Bessel functions which is valid when the surface wave phase velocity is very close to the speed of light c. This condition is fulfilled when either the dielectric thickness is much smaller than the wire radius, $d \ll a$, or when $d \lesssim a$ and the radius a is very small compared with the wave length [16]; both of these criteria are satisfied for our G-line setup.

Solving Eqs. (3) and (5) will give the surface wave parameters γ_0 and γ_d as a function of frequency ω, which we can then use to study the free-field solutions $B_\phi \sim E_r \sim H_1^{(1)}(\gamma_0 r)$. In particular, we would like to compare these fields in the vicinity of the wire to the known $1/r$ behavior of a relativistic electron beam. We did this for our G-line design by numerically solving (3) and (5) in *Mathematica* for a wire with inner radius $a = 143.5$ microns that is coated with 20 microns of a $\epsilon_r = 3.5$ dielectric film (so that $b = 163.5$ microns). We found that at 10 GHz the deviation of E_r and B_ϕ from the desired $1/r$ behavior was less than 10% out to a distance of 12.3 mm, while at 5 GHz the discrepancy at 11 mm was $\sim 2.5\%$. Since the nominal radius of the tested APS-U vacuum chamber components is 11 mm, the surface waves appropriately model the $1/r$ properties of the electron beam over the 1 to 10 GHz frequency range of our measurement.

We also verified this $1/r$ behavior of the G-line with CST simulations. Figure 2 shows a contour plot of the magnitude of E_y at the plane $x = 0$ for the frequency of 2 GHz, while Fig. 3 plots the radial electric field extracted from this contour plot on a log-log scale, showing that the field falls off as $1/r$ out to the radial distance of about 65 mm, which agrees quite well with the semi-analytic result of 66.6 mm. Note that 65 mm also happens to be the size of the

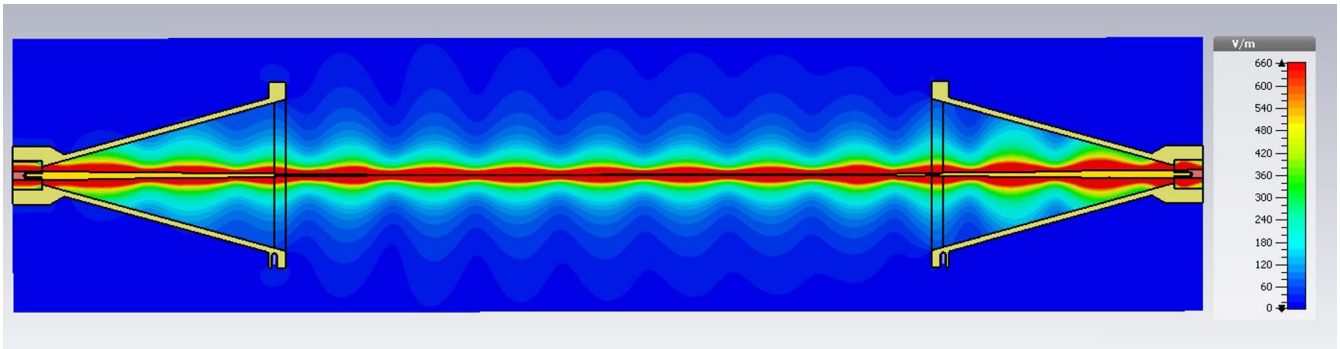

FIG. 2. Contour plot obtained from CST simulation showing the localized electric fields, y-component, at 2.0 GHz in the G-line.

launching and receiving horns, and that at 2 GHz ~ 95% of the surface wave energy is contained within a cylinder of the cone radius. At 1 GHz about 80% of the field energy is in this same distance, giving sufficient launching and receiving efficiency over the entire 1 to 10 GHz range.

B. Description of the G-line setup designed at Argonne National Lab

The previous section described steady-state surface waves that could in principle be used for impedance measurements. Goubau [27] showed that these waves can be efficiently excited using launching and receiving "horns" that are tapered, conical structures which serve to minimize the impedance mismatch between the coaxial cables and the single-wire transmission line. In other words, the horns effectively convert the TEM mode of the input coaxial cable into the fundamental TM surface wave mode of the dielectric coated wire and back again [14]. These horns are actually transmission line tapers matching the coaxial cable impedance (50 Ω) to the wave impedance of the Goubau line [28,29]. A properly designed horn will limit coupling to higher-order modes that can lead to deviations in the mode wave-front [22,27]. The diameter of the horn opening is determined by the largest effective mode size that one wants to transmit (i.e., the mode size at the minimum frequency of interest), while the ratio of the diameter to length should be small enough for smooth matching, but is ultimately limited by reasonable length constraints; previous works have chosen this ratio in the range between 0.4 and 1.0 [14,27].

The G-line system designed at Argonne National Lab is shown in Fig. 4. The launching and receiving horns are made of aluminum with an opening diameter of 130 mm that allows for good coupling to surface waves above 1 GHz, and a tapered length of 210 mm to provide good impedance matching; these dimensions are similar to those described by Goubau in his seminal paper [16] on surface wave propagation. Within each horn is a central brass taper that connects the coaxial cable to the central wire. To smoothly match the impedance, the brass taper is transitioned from its maximum diameter of 7.35 mm at the coaxial line to its final diameter of 1.05 mm at the wire over a total of six 1.05 mm steps. The brass tapers are covered in Fig. 4 by teflon spacers (the white circles at the opening of each horn), which serve both to position the brass taper along the central axis and to help to damp higher order modes. Finally, the brass tapers are connected to the single wire transmission line, which we have chosen to be a 927 mm long magnet wire with dimension of 29 American Wire Gauge (diameter ~287 microns) that has a 20 μm polyimide coating with dielectric constant of 3.5. Theoretically, the G-line surface waves have a lower

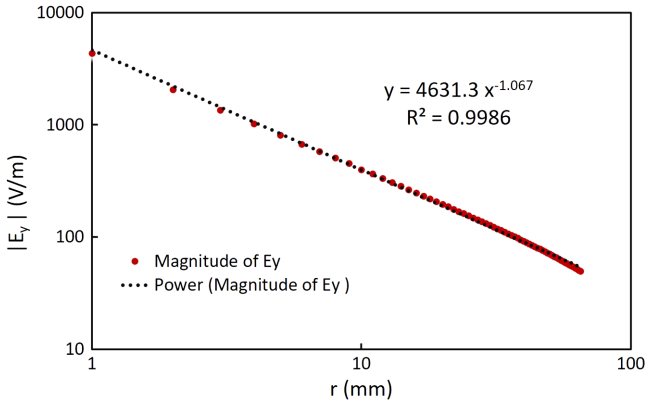

FIG. 3. Graph showing E_y from contour plot with radial distance (red dots), and a fitted line (black dots) to the field data displaying $1/r$ characteristic of a relativistic particle beam.

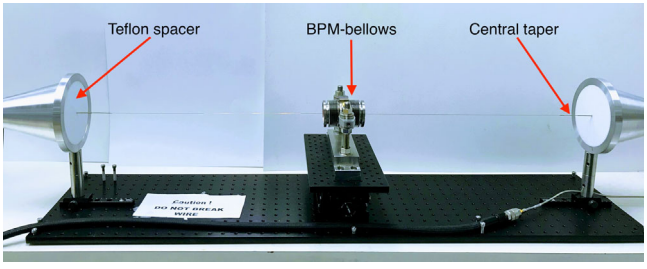

FIG. 4. Experimental G-line setup designed at the Argonne National Laboratory to measure the coupling impedance of a DUT.

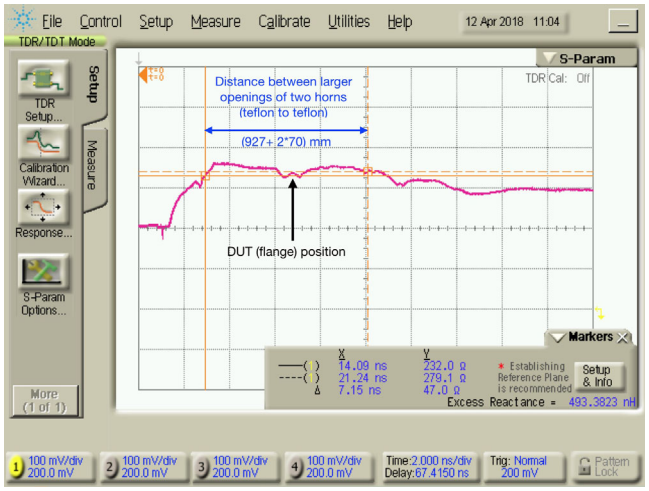

FIG. 5. A screen-shot image showing the TDR measurement (S_{11} plot with respect to time) at the single ended mode by placing a DUT in the middle of the G-line setup and terminating the receiver horn with a 50 Ω load.

cut-off frequency of zero, but the launcher geometry introduces certain practical limitations that for our geometry set a lower frequency of around 0.5 GHz. Simulations have shown that this should be sufficient for the APS-U structures, while the 10 GHz maximum, which is set by the $1/r$ characteristics of the chosen magnet wire, is well above the 3 sigma frequency $f \approx 6.8$ GHz set by the APS-U minimum bunch length of 50 ps. In addition, the quality of coaxial cables and connectors that we have are not good enough to measure above 10 GHz due to very high attenuation of rf-signals.

Our first test of the G-line performance was to measure the time domain reflectometry (TDR) to evaluate the impedance matching from the coaxial cable to the wire and through a DUT. TDR measures the reflection coefficient (S_{11}-parameter) with respect to time, from which one can determine the degree of impedance mismatch at any point along a transmission line. Our TDR measurement is in Fig. 5, which shows a smooth impedance transition from the 50 Ω coaxial cable to that of the dielectric coated wire, and then to the characteristic impedance of the DUT at the middle of the G-line. There are small variations where the DUT is located which we believe can be attributed to mode conversion from TM to TEM modes at the entrance and back again at the exit. As we discuss in the next section, use of the reference sleeve should normalize out these effects. We do not completely understand why the TDR measurement indicates an impedance above 50 Ohm after the receiver cone. One potential explanation is related to the fact that multiple changes in impedance along a line result in multiple reflections that need to be taken into account [30]. For example, if the impedance changes from, say, 50 Ω to 100 Ω and then back to 50 Ω, the measured reflection from the second impedance step would be smaller than that of the first one due to reflections on the return path at the first step. Hence, the inferred impedance of the second transition would be greater than 50 Ω, and similar (but more complicated) effects will occur with the smooth impedance transitions to and from the horns. We plan to investigate this further.

Theoretically, the impedance is a function of frequency so that impedance mismatch cannot be fully avoided for all measurements, especially in the traditional coaxial method, where it increases due to additional capacitive behavior observed in the resistive circuit used for impedance matching at higher frequencies; nevertheless, it can be minimized using the G-line setup as the reference sleeve normalized out this mismatch.

C. Impedance measurement procedure using the G-line system

Experimentally determining the impedance of any vacuum component requires inserting the device under test (DUT) into the G-line test apparatus, calibrating the network analyzer with an appropriate reference, and measuring the response of the DUT. For the first step, we place the DUT directly between the two horns, thread through the magnet wire, and solder the wire to the horns. We then position the DUT vertically with knobs and horizontally with positioning screws so that the wire passes directly down the chamber axis, and finally fix the DUT to the optics board with holding clamps and screws.

Once the DUT is properly positioned, we set the reference by inserting a flexible, 0.1 mm thin brass sleeve, shown in Fig. 6(a). This sleeve forms an effective reference chamber by virtue of its precise fit and good rf contact with the nominal 22 mm APS-U chamber as shown in Fig. 6(b). Furthermore, the sleeve can be easily inserted and removed without disconnecting the central wire or disturbing the experimental setup. Having established the reference, we then calibrate the network analyzer so that the S_{21}-signal becomes completely flat, gently remove the sleeve, and then record the S_{21} parameter of the DUT. This measurement yields the normalized response $S_{21}^N = S_{21}^{\mathrm{DUT}}/S_{21}^{\mathrm{REF}}$ that we can then convert to an impedance using appropriate formulas, as we discuss later. Our measurements will focus

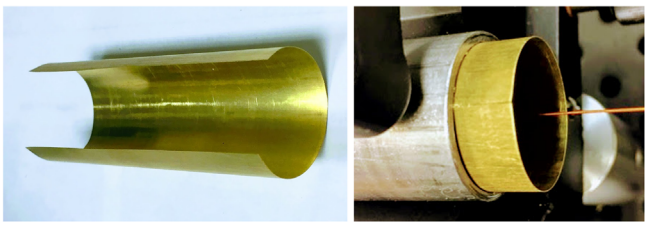

(a) (b)

FIG. 6. Brass sleeve; (a) without inserting into DUT, and (b) partially inserted into the DUT of a nominal APS-U diameter of 22.0 mm.

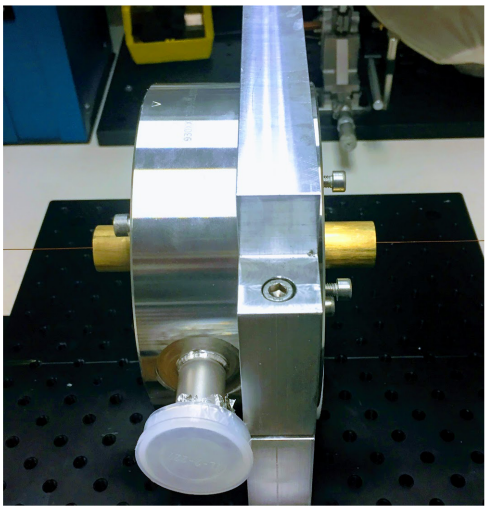

(a)

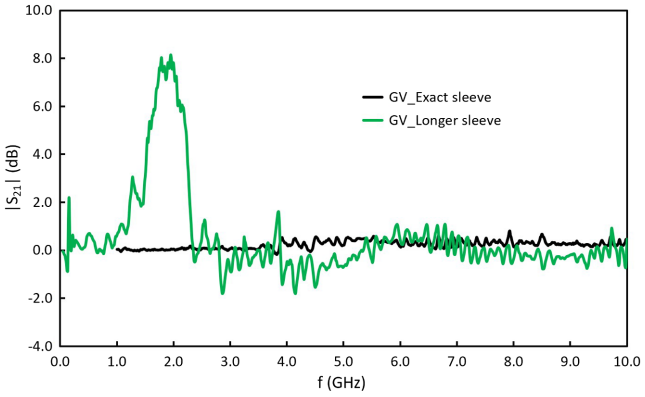

(b)

FIG. 7. (a) A prototype gate valve for the APS-U with a brass sleeve (yellowish cylinder) longer than its length. (b) Comparison between the APS-U gate valve response for two different sleeve lengths; green curve represents a response for a longer sleeve, and the black curve indicates the same response while using an exact sleeve.

on the longitudinal impedance, both because we are particularly concerned with the potential difficulties associated with rf heating, and because our impedance modeling [31] predicts that the primary contribution of these vacuum components is to the longitudinal microwave instability in the APS-U.

During the course of our measurements we found that their accuracy is significantly impacted by the choice of reference sleeve. In particular, we discovered that using a sleeve whose length precisely matches that of the DUT is imperative to obtain reliable results. Our initial thought was to use a common sleeve for all chambers, but we observed sharp, unphysical positive peaks (sometimes referred to as "overshooting") of the S_{21}-parameter at low frequencies when the sleeve protruded outside the DUT. Figure 7(a) shows a picture of one case where the sleeve was too long, while Fig. 7(b) compares measurement with this setup

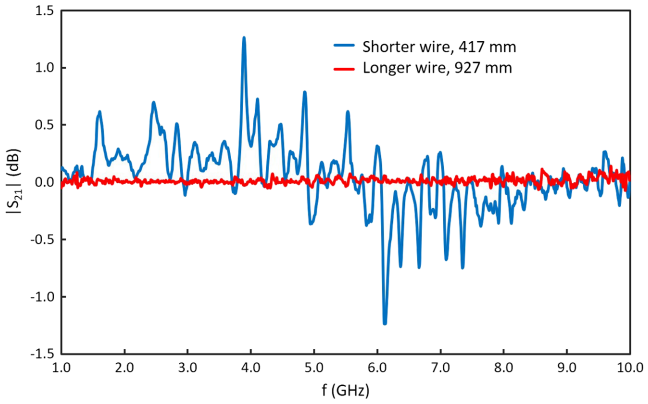

FIG. 8. Comparison between the measured data for a DUT for two different gap spacing between G-line cones; the blue curve corresponds to 417 mm, and the red curve corresponds to 927 mm.

(green line) to that when the sleeve length matched that of the gate valve (black). We see that choosing the appropriate reference sleeve eliminates the unphysical overshooting response, resulting in an accurate measurement of the S_{21}.

In addition, we found that the systematic error of the G-line measurement becomes undesirably large if the launcher cones are too close to one another. These findings are consistent with the simulation results of Ref. [19], who found that the wire needs to be sufficiently long to insure good launching and receiving efficiency. This is because the G-line needs sufficient space between the cones and the DUT for the surface waves to fully develop. Increasing the wire length further can in principle lead to additional improvements, but any benefit must be weighed against other sources of error and how much lab space can be occupied. Figure 8 illustrates this point by comparing the measured response from a flange and gasket when the two G-line cones are 417 mm apart (blue line) to that when the cones are placed 927 mm apart (red line). In this case we find that increasing the length between the cones by a factor of 2 decreases the systemic error by a factor of 10. While the reduction in noise was not as dramatic for other cases, we did find at least a factor of 2 noise reduction for all other APS-U vacuum components.

III. BENCHMARKING OF THE G-LINE METHOD

We are among the first groups to use a two-horn Goubau line setup to measure the coupling impedance of accelerator vacuum components. Hence, we believed it was important to first test its performance using a relatively simple and well-understood cylindrically symmetric cavity. The dimensions were chosen to match those of the cavity formed when two quick con-flat (QCF) flanges are joined without any gasket: the input and output cylindrical pipes have 11 mm radii and are 90 mm long each, while the cavity formed by the flanges is 2.54 mm long with a radius of 24.2 mm. The CAD model of this benchmarking cavity is shown in Fig. 9(a).

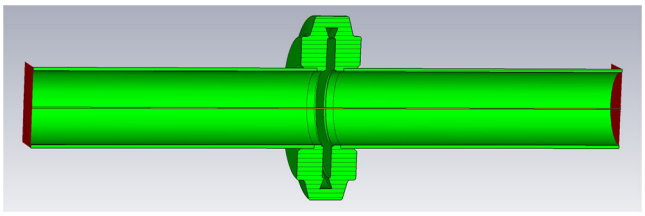

(a)

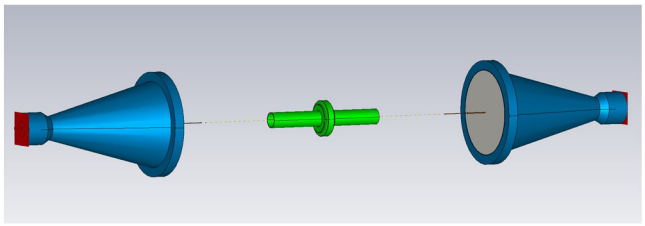

(b)

FIG. 9. Two separate CAD models to simulate S_{21}-parameter of a 2.54 mm wide pillbox type cavity: (a) without the G-line system, where the central black line is the dielectric coated copper wire, and (b) the same cavity in the G-line system.

A. Benchmarking the S_{21} parameter

Our first step was to determine whether the launching and receiving horns introduced any artifacts in the measurement. To do this, we compared the simulated S_{21}-parameter from a simulation of the entire G-line test fixture to that of a simplified simulation that only included the central wire inside the DUT. A 2.54 mm wide pillbox type cavity was chosen as a DUT and is formed by joining two flanges together without putting any gasket in between. Both simulations were performed using the transient solver of CST Microwave Studio, and Fig. 9 shows the CAD designs used for the simulation without (a) and with (b) the G-line system. Both simulations include the dielectric coated wire, and Fig. 9 also indicates the positions of the input and output waveguide ports by the red planes.

We compare the normalized S_{21}-parameters obtained from the two simulations in Fig. 10. The red curve plots the normalized data obtained from the simulation of the full G-line system, while the black curve plots the same using the simplified DUT model. We see that the agreement is quite good, and significantly that the position of the resonance peaks in both cases lies at the same frequency. This shows that the G-line launching and receiving setup does not introduce any artifacts, and that we can in the future compare experimental results to the simplified simulations that only include the DUT. This allows for simulations that have improved numerical resolution for a reasonable computational time.

The next step was to compare the benchmarked simulation results to those obtained from experiment. As mentioned previously, we made the experimental cavity by joining two QCF-flanges together with a chain-clamp as shown in Fig. 11(a), after which we wrapped the outer

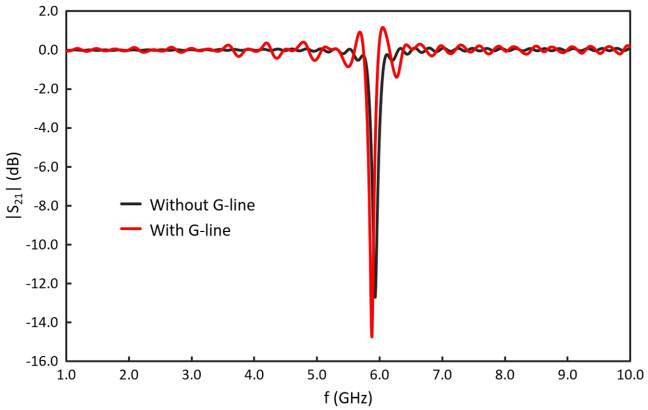

FIG. 10. Simulated plots comparison to benchmark the G-line system for a 2.54 mm wide stainless steel 316L pillbox type cavity with and without G-line setup, where the red curve represents normalized S_{21}-data with G-line setup, and the black curve represents the normalized data without the G-line system.

circumference with copper tape to ensure good rf contact. We compare the measured and simulated S_{21} parameter in Fig. 11(b), where the black curve represents the simulated response of the cavity, and the green curve is the measured one with G-line setup.

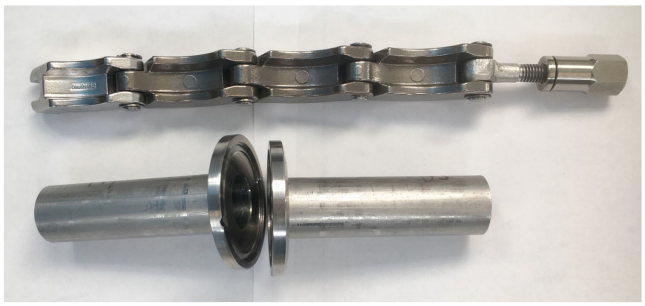

(a)

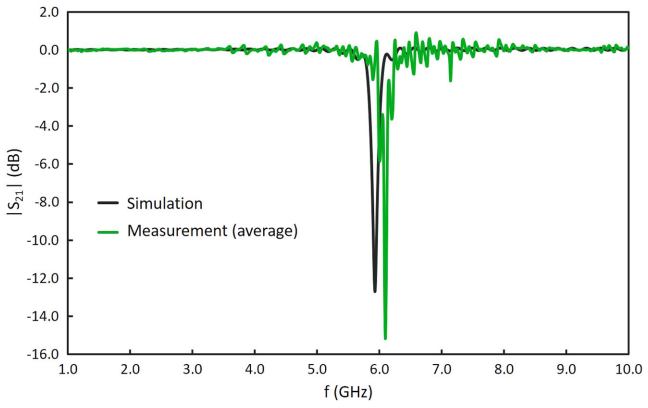

(b)

FIG. 11. (a) Chain-clamp along with two QCF-flanges to form a bench-marking cavity. (b) Measured data comparison with simulation, where the green curve represents normalized S_{21}-data with the G-line setup, and the black curve represents simulated S_{21}-data without the G-line.

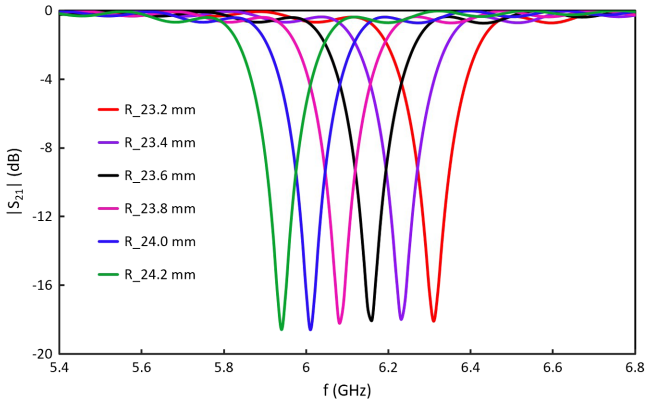

FIG. 12. Resonance peak positions found from CST simulation for a 2.54 mm wide perfectly conducting pillbox cavity with different radii. The green, dark blue, magenta, black, purple, and red curves represent the radii of 24.2 mm, 24.0 mm, 23.8 mm, 23.6 mm, 23.4 mm, and 23.2 mm respectively.

We observe that the measured and simulated resonance peaks are very similar, except that the frequency of measured peak is about 0.1 GHz higher (∼1.7%). Since the basic theory of pillbox cavities predict that the frequency of the fundamental TM_{010} mode varies inversely with the radial size of the cavity, we hypothesized that the difference in the position of the resonance could be explained by small geometric differences between the simulated and measured cavity. We then tested the sensitivity of the frequency to the geometry by varying the radial dimension of the cavity in our CST simulations; the resulting S_{21}-parameters are shown in Fig. 12, which clearly depicts the $1/R$ dependence of the resonance peak position. From these simulations we see that a ∼0.2 mm difference in the cavity radius could account for the discrepancy between measured and simulated frequency position of the cavity resonance. After these simulations we did remeasure the cavity radius with Vernier calipers, but did not find any such discrepancy in the dimensions. We therefore consider the 0.2 mm (or ∼0.1 GHz) to quantify how accurate the G-line is, and how much confidence we should attribute to our measurements.

B. Impedance of the benchmark cavity

There are several formulas [8,9,32,33] of differing domains of applicability that relate the S_{21}-parameter to impedance. The benchmarking cavity can be approximated as a lumped impedance structure since its width is much less than the diameter of the beam pipe, so that the Hahn-Pedersen (HP) formula [8] applies:

$$Z_{\parallel}^{HP}(\omega) = 2Z_c\left(\frac{1-S_{21}^N}{S_{21}^N}\right). \tag{6}$$

Here, Z_c is the characteristic impedance of the coaxial cable (reference pipe in our case), which we approximate

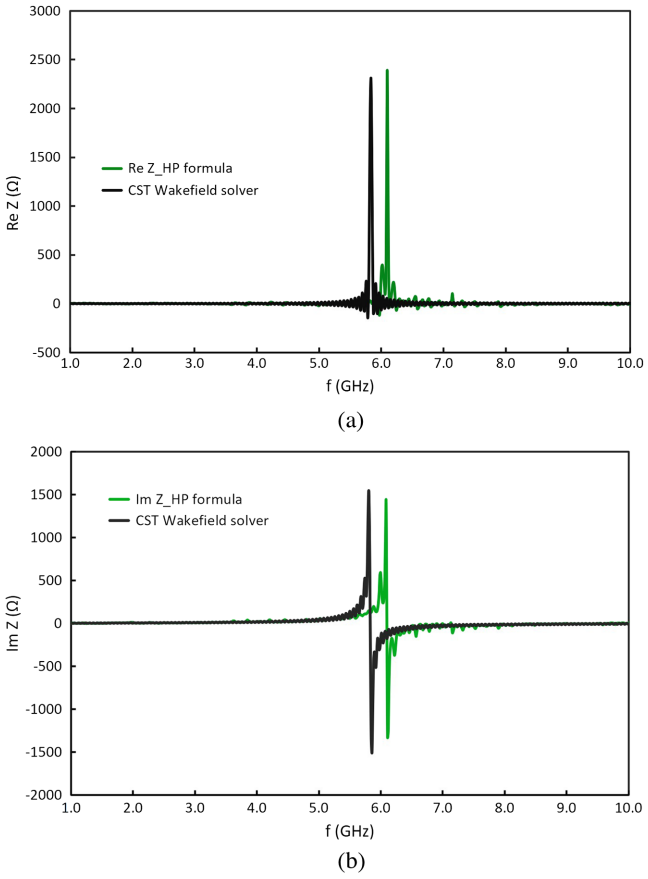

FIG. 13. Comparison between the measured and simulated impedances: (a) real part, and (b) the imaginary part for a bench marking cavity. The black curve represents the simulated impedance using the CST wakefield solver, while the green curve indicates the measured impedance calculated from the HP formula.

using the loss-less formula in air, $Z_c = \frac{Z_0}{2\pi}\ln(d_1/d_2)$, where $Z_0 \approx 120\pi\ \Omega \approx 377\ \Omega$ is the impedance of free space, d_1 is the inner diameter of the beam tube, and d_2 is the outer diameter of the central conductor. There are some concerns regarding the validity of the lumped impedance formula Eq. (6), since the presence of the wire perturbs cavity fields and leads to a certain detuning, but for the micron sized wire that we have used it works relatively well [34].

We also compared this calculated impedance with simulation results obtained using CST Wakefield solver. The wakefield was simulated for 5000 mm behind the exciting charge to insure sufficient spectral resolution of the corresponding impedance. We used CST Wakefield solver to directly obtain the impedance partly to improve accuracy and partly to verify our conversion of S_{21} to impedance Eq. (6). Figure 13 shows the comparison between real and imaginary parts of the measured and simulated impedances, where the green curve represents the measured response and the black curve represents the simulated response. The comparison shows that the real and imaginary parts of the

measured and simulated impedances looks very similar except for a slight shift in resonance peak position which accounts for ~0.4 mm discrepancy in the radial size of the cavity in this case. We had observed ~0.2 mm shift while comparing measured and simulated S_{21}-parameter, and the additional 0.2 mm shift may be due to the perturbation produced by the central conductor to represent particle beam in the measured data since the wakefield simulation does not have this central conductor.

It is clear from the above comparison between the measured and simulated data that the Goubau line provides a novel impedance measurement technique that is powerful and accurate. The impedance formula given by Eq. (6) is derived for a loss-less transmission line. Although the G-line system has some losses, the distance between the cones is sufficiently small such that we can approximate it as a loss-less transmission line and the impedance formula that we used are valid [8,18].

IV. MEASUREMENTS OF CRITICAL VACUUM CHAMBER COMPONENTS

In this section we describe the G-line measurements and impedance analysis of several critical APS-U vacuum components. These components were selected from the APS-U impedance model [31], which in turn was developed by identifying and simulating impedance contributions from engineering drawings. The primary goal of our bench measurements is to ensure that all components will be subject to small levels of rf heating in the APS-U ring, while at the same time verifying our impedance calculations as best as possible.

A. rf gaskets for QCF flange

Because the APS-U vacuum system calls for ~2000 flanges, their design must be reliable and contribute as little impedance as possible. Standard vacuum gaskets leave a large cavitylike structure between the 22-mm diameter chamber and the vacuum-sealing knife edge as discussed in the section of benchmarking, which would lead to an undesirably low threshold current for the longitudinal microwave instability and potentially problematic levels of rf heating. Therefore, another design is required that can economically balance good vacuum performance with ease of installation and impedance cost. Of three initial designs one was rejected due to the difficulty of its installation, while the remaining two are shown in Fig. 14. The first design on the left is composed of two parts: an outer ring into which the knife edge bites for the vacuum seal (not shown), and an inner ring whose beryllium-copper comb provide the rf shield. The second gasket on the right is a single piece of annealed copper whose outer area allows for the vacuum seal at the flange knife edge, while having an inner ring that is designed to provide rf contact at (or near) the nominal chamber radius. We present measured results

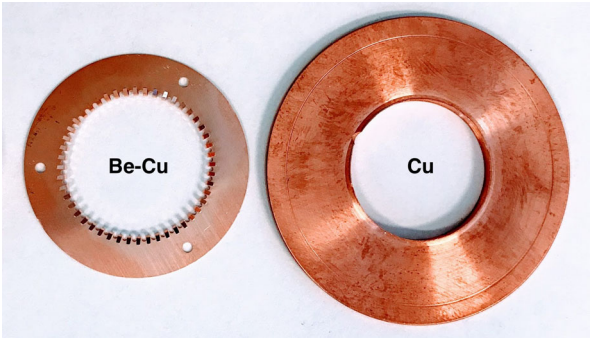

FIG. 14. Gasket options for the APS-U lattice; A beryllium-copper comb rf-gasket (left), and a single conflat copper gasket (right).

for these gaskets including their analysis in the following subsections.

1. Beryllium-copper comb rf-gasket

This gasket achieves its rf-seal using thin and elastic beryllium-copper fingers which we refer to as a comb in this paper. While this gasket requires an additional outer gasket for the vacuum seal, installation is simplified by screwing the gasket into the flange wall as shown in Fig. 15(a). Furthermore, the compressible fingers of this

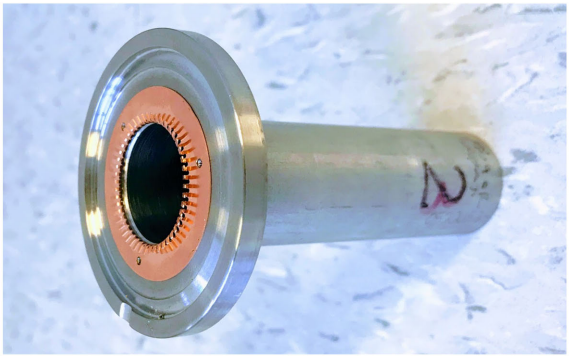

(a)

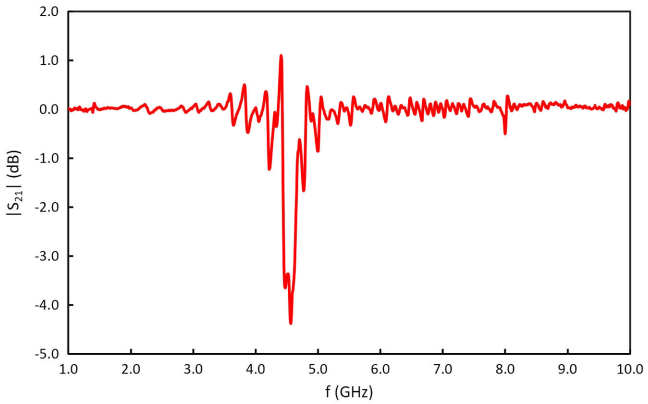

(b)

FIG. 15. (a) A QCF flange with the beryllium-copper comb rf-gasket. (b) Initially measured S_{21}-data for this gasket design.

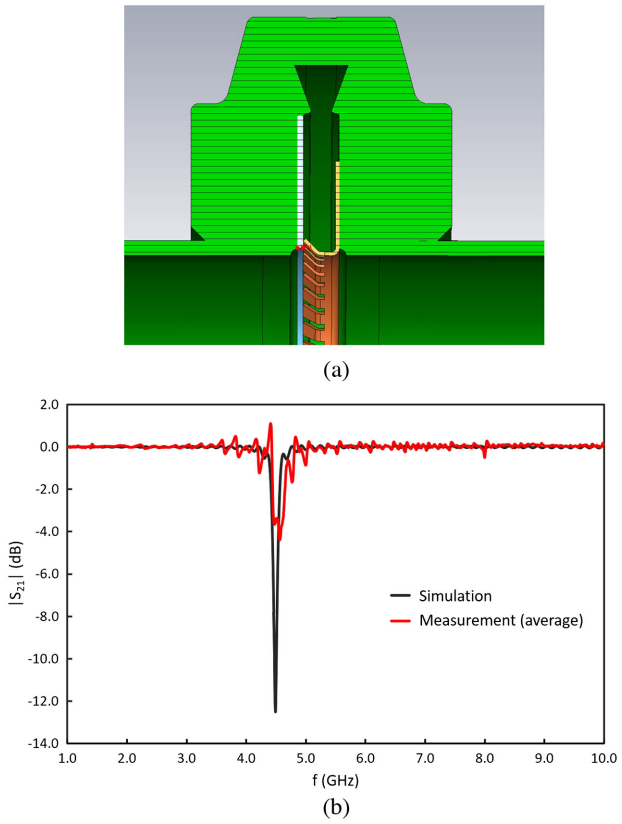

FIG. 16. (a) Plane view of a CST CAD model showing a 0.4 mm longitudinal gap (cyan color) between the Be-Cu comb rf-gasket and the side wall of QCF flange. (b) Comparison between measured (red curve) and simulated response (black curve) due to this 0.4 mm gap.

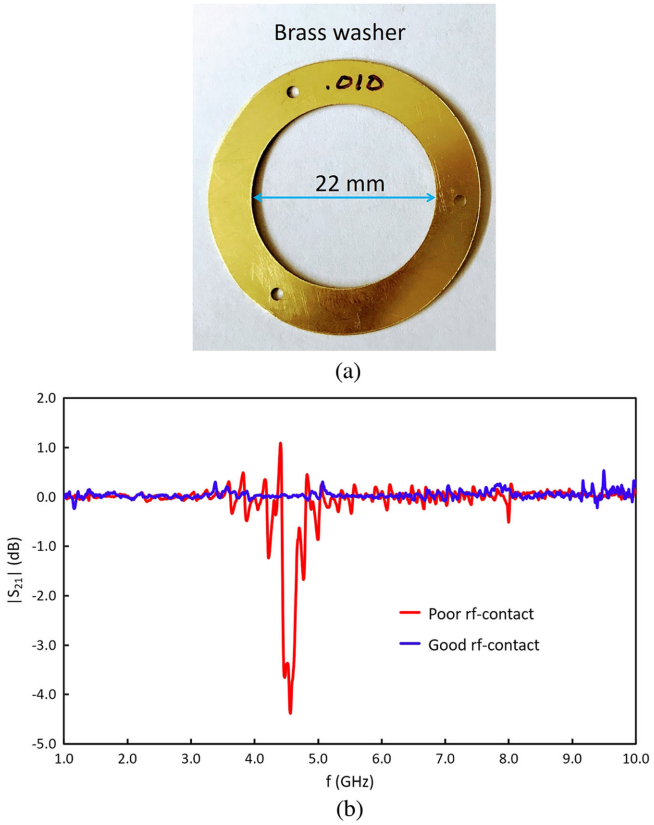

FIG. 17. (a) A typical brass washer used to fill the gap between rf-fingers and the flange wall. (b) Comparison between the measured responses of the beryllium copper comb gasket with good rf-contact (dark blue curve), and poor rf-contact (red curve).

design alleviates fears of a poor vacuum seal and/or the introduction of virtual leaks.

Surprisingly, our initial S_{21} measurements of the beryllium-copper rf-gasket showed a resonance peak between 4 and 5 GHz as shown in Fig. 15(b), which was in contrast to our simulation predictions. After a careful investigation of this gasket, we found that the comb fingers were not fabricated according to specifications: the fingers were shorter than designed, which led to a ~0.4 mm gap between the fingers and the flange wall.

To verify that this lack of rf-contact was a main cause behind the observed resonance peak, we added a 0.4 mm gap into the CST model as shown by the cyan colored area in Fig. 16(a), and compared the new simulation result with the measured one. Figure 16(b) shows this comparison, where the red curve represents the measured data and the black curve represents the simulated data. Comparison shows both resonance peaks at the same frequency though simulation overestimates the peak amplitude.

We then wanted to show that the observed resonance peak could be eliminated by making a good rf-contact between the rf-fingers and the flange. For this, we filled the rf-gap with the brass washers, having the same internal diameter as that of nominal APS-U beam pipe of 22 mm, one of which is shown in Fig. 17(a) and remeasured the transmission coefficient. In this case, we found a nearly flat S_{21}-parameter shown as the dark blue line in Fig. 17(b).

Finally, we proceed to compute the complex impedance from the measured S_{21}-parameter for Be-Cu comb gasket when there was a gap between the gasket and the flange wall, which we compare to simulation results from CST wakefield solver in Fig 18. The red line is computed from the experimental data using the Hahn-Peterson formula for the lumped impedance structure, while the black line is simulated impedance obtained from CST. The measured and simulated results are in good agreement with each other, and all show an impedance characteristic of a cavity that is qualitatively similar to the benchmark cavity of the previous section.

We have seen that the comb gasket could be suitable from an impedance perspective provided it has proper tolerances to ensure good rf-contact. On the other hand, the APS-U is looking to limit its reliance on beryllium-copper,

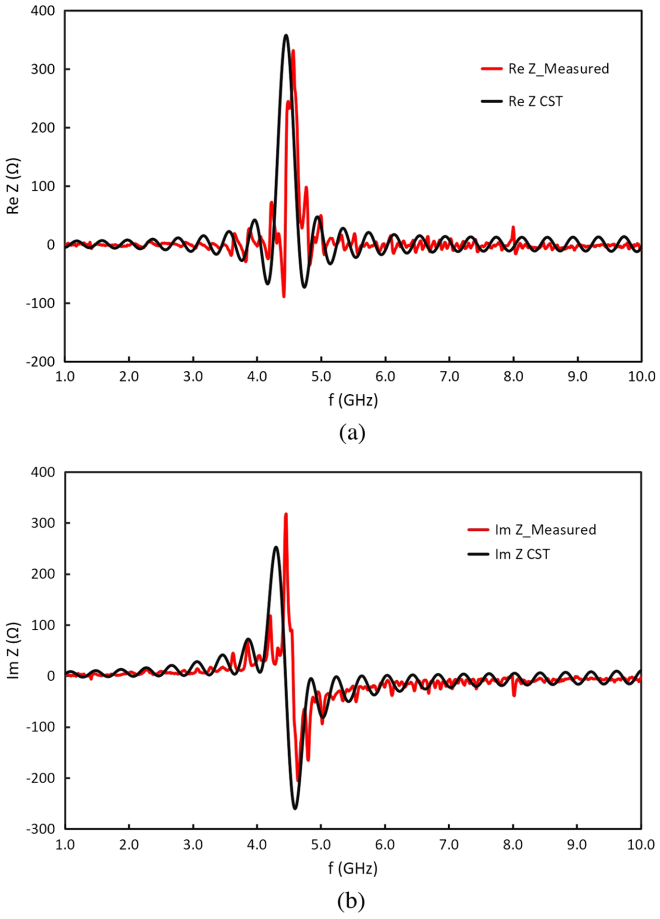

FIG. 18. Comparison between measured and simulated impedances for the Be-Cu rf-gasket: (a) Real part, and (b) Imaginary part. The red curve represents measured plot using the HP formula, and the black curve represents simulated plot using CST wakefield solver in both (a) and (b).

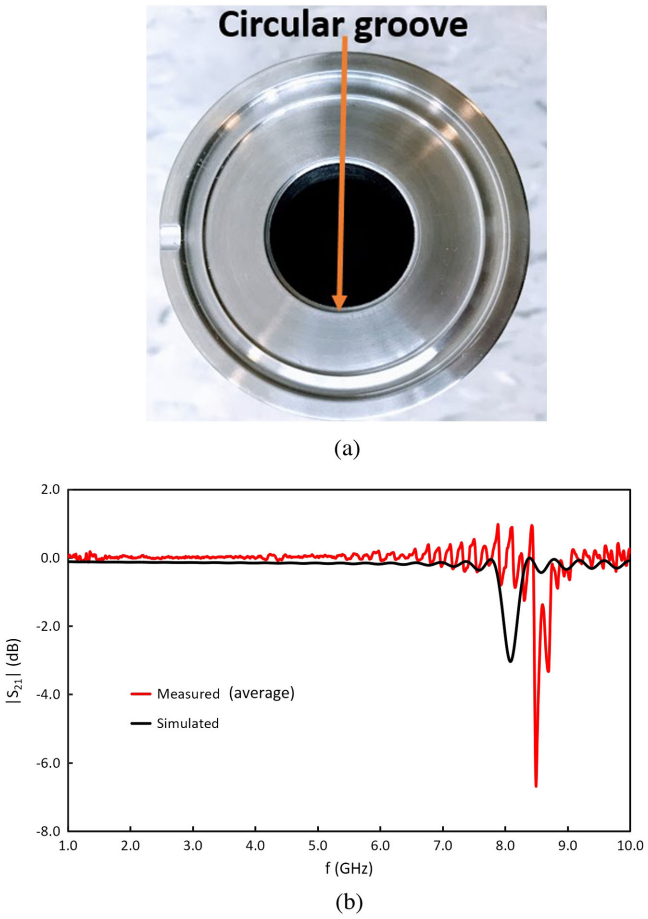

FIG. 19. (a) A QCF flange fabricated without proper tolerance showing a circular groove at the joint surface between flange and beam pipe. (b) Comparison between measured (red curve) and simulated (black curve) responses for the single conflat gasket with flanges having grooves.

and there are some lingering concerns regarding its ease of installation. Hence, at present this gasket is not the first choice.

2. Single conflat gasket

The single conflat gasket is designed to provide both rf-and vacuum seals. This gasket has two triangular-shaped edges at its inner diameter, called A-joints or lips, which provide an rf-contact between gasket and flange. The circular knife-edge on the inner surface of the flange bites the gasket near its outer diameter and hence provides vacuum seal. The A-joint contains a couple of small notches (holes), which allow vacuum pumping between the inner gasket ring and the outer knife edge.

The initial measurement of transmission coefficient for the single conflat gasket also showed a resonance peak between 8 GHz and 9 GHz plotted with the red curve in Fig. 19(b), which was not predicted by CST simulation. After disassembly we found a small circular groove at the inner welding surface between the flange and the beam pipe as shown in Fig. 19(a). These two grooves prevented the gasket from making a good rf-contact with the flange, which in turn led to electromagnetic coupling between the beam pipe and the flange cavity.

We measured the radial dimension of the circular groove to be 0.5 mm, and estimated its width to be approximately the same. We then included this cavitylike groove in the original CAD design and reran the simulation to cross check our previously measured result. In Fig. 19(b) we show that the measured resonance peak (red) is similar to that observed in the simulation (black), except the amplitude of the simulated peak is smaller and at a slightly lower frequency than that measured. Additional simulations showed that a 0.5 mm difference in the radial position of knife edge can explain this discrepancy; we observed a similar situation for the benchmarking cavity in Section III.

Later on, we tested the performance of the single piece gasket using the properly designed flange without circular groove shown in Fig. 20(a). The first test used a gasket whose rf lip (A-joint) was chosen to be 2.7 mm wide.

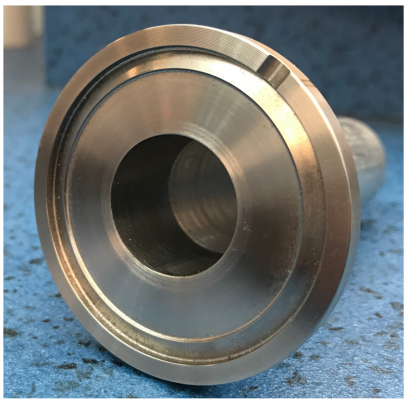

(a)

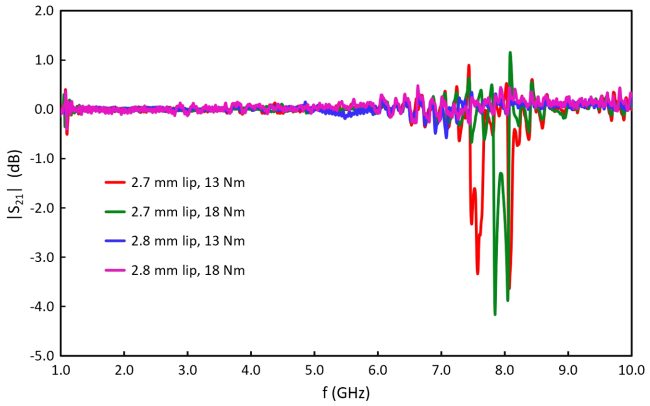

(b)

FIG. 20. (a) An appropriately toleranced flange. (b) Measured responses of the conflat gasket with a slightly small rf lip (red and green), and a suitably sized rf lip (blue and magenta).

Unfortunately, measurements for the G-line showed that this was insufficient to provide good rf contact as shown by the red and green lines in Fig. 20(b). The rf lip width was then increased to 2.8 mm, which we found both did not interfere with the vacuum seal while adequately shielding the flange joint as seen by the blue and magenta lines in Fig. 20(b). In addition, we found that increasing the chain clamp torque from 13 Nm to 18 Nm eliminated a small, low-Q resonace near 5.5 GHz.

The single conflat gasket has since been adopted as the flange gasket of choice, because we have found it to provide suitable vacuum and impedance performance, while being somewhat easier to install and maintain.

B. BPM-bellows assembly

The APS-U has stringent demands on the mechanical stability of the beam-position monitors (BPMs) so that they can meet tolerances of $\lesssim$1 micron rms drift per week. Any local heating can potentially displace the buttons and overwhelm these tolerances. In addition, the BPM-bellows assemblies contribute the second largest longitudinal impedance for the MBA lattice. Therefore, we tested the impedance cost of the BPM-bellows assembly to understand all sources of heating including that of beam-induced rf-heating.

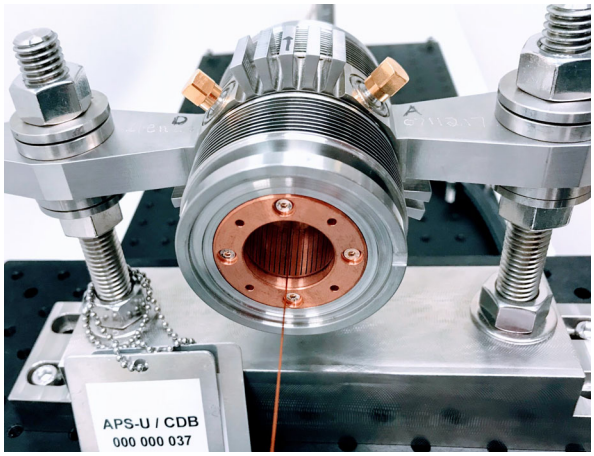

FIG. 21. A real picture of a prototype BPM-bellows assembly for the APS-U.

Figure 21 shows a real image of a prototype BPM-bellows assembly designed for the APS-U. The BPM is comprised of four signal pick up buttons arranged symmetrically at a 12 mm distance from the beam axis. Each button is 2 mm thick and 8 mm in diameter, while the BPM pin dimensions have been tailored to best match the characteristic impedance to 50 Ω. The lowest resonance mode due to the button geometry is expected to have a frequency of about 11 GHz.

We plot the measured response for BPM-bellows assembly as the green curve in Fig. 22(a), which shows no resonance peaks over the entire 10 GHz range. This agrees with the CST simulations plotted as the red curve in the same Fig. 22(a). The measured response is within the noise level of the Network Analyzer in the frequency range of 1 GHz to 6 GHz, however it increases by nearly a factor of 2 in the frequency range of 6 GHz to 10 GHz. The RMS value of the measured data is found to be 0.07 and 0.23 in the frequency range of 1 GHz to 6 GHz and 6 GHz to 10 GHz, respectively.

To figure out the possible cause behind the increased in amplitude of the measured response beyond 6 GHz, we remeasured the BPM-bellows response after shifting its longitudinal position by 10 mm with respect to its initial central position. The resulting comparison is shown in Fig. 22(b), where the black curve is the response when the BPM-bellows is placed at the center between the two G-line horns, and the red curve is the response when it is shifted longitudinally by 10 mm. The comparison shows that the response is shifted by $\sim 180^0$ in phase above 5 GHz. In another words, the frequency position of the peaks and valleys of the S_{21}-parameter change only when we make change in DUT's longitudinal position along the G-line by a small amount. Since this does not change any of the

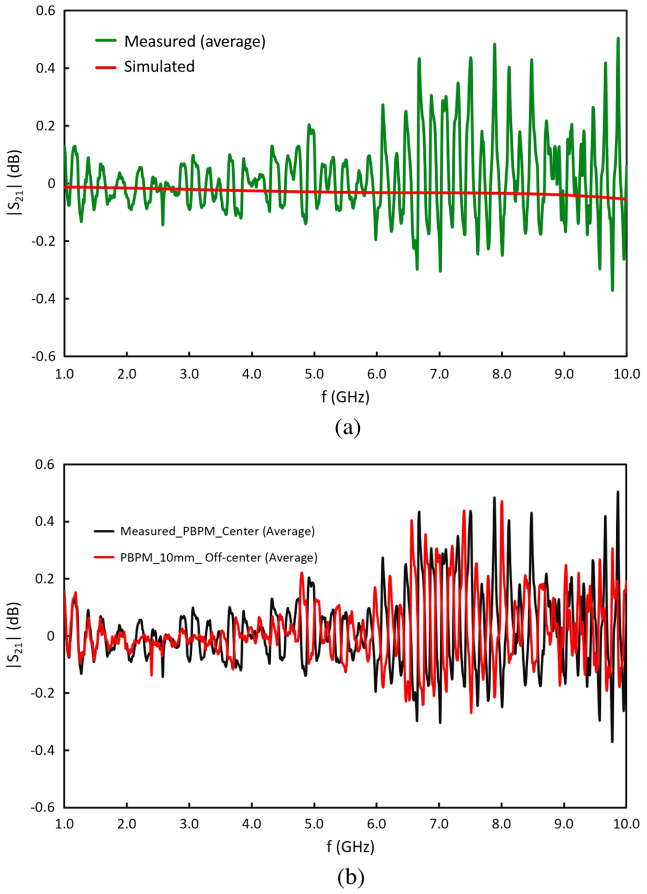

FIG. 22. (a) Comparison between measured, and simulated S_{21}-parameter of a prototype BPM-bellows assembly, where the green curve represents the average data of three measured trials, and the red curve represents the simulated data. (b) Comparison between the measured responses of the same BPM-bellows assembly; initial central position (black curve), and 10 mm off longitudinally with respect to initial central position (red curve).

internals of the DUT, the signal is not purely noise, and seems to indicate that it is related to reflections and distortions associated with the placement of the DUT itself. These effects may ultimately limit the sensitivity of the G-line impedance measurement, and warrant further analysis in the future.

C. Other components

We have also measured the impedance of other APS-U vacuum chamber components including a gate valve liner and a pumping cross. The details of these components and their measurement results can be found in Ref. [35]. Here, we merely give an overview of the components and summarize the results.

An important part of the APS-U gate valve is its rf-liners, which ideally serve to electromagnetically shield the electron beam from the large opening that houses the gate valve doors. The gate valve liners have a 20 micron-thick silver coating on top of stainless steel liners. The whole body of the gate valve is made out of stainless steel 316L. Simulation of the impedance caused by these rf-liners is challenging due to their intricate geometry, and our experience at the present APS has shown that gate valves can experience significant rf heating. Hence, careful design and rf measurements for future gate vale liners are important. For the prototype APS-U liner, we found that the measured transmission coefficient showed no observable resonance peaks below 10 GHz as we anticipated from CST simulation.

The APS-U pumping cross will use a total of six vented slots, three along the top and three along the bottom, which will act as a beam screen from the ion pumps. The pumping cross has the same 22 mm internal diameter as that of nominal APS-U beam pipe, and it will be welded into a 57 mm inner diameter cross body which is again welded to the 316 L stainless steel flanges. Both the pumping cross and the cross body are made from 6063 aluminum. An ion pump will be connected to one of these flanges to maintain vacuum pressure. The measured response of the pumping cross also showed a flat S_{21} over the entire 10 GHz range as predicted by computer simulation.

V. CONCLUSION

We have described how the novel G-line can be used to measure the coupling impedance of a wide array of vacuum components. After a brief theoretical background we have explained our measurement procedure in some detail, including the measurement setup and proper definition of a reference, advantages over the traditional coaxial wire method, and our experience regarding how to reduce systematic experimental error that we learned over the course of the measurements. After benchmarking the G-line measurement technique both from simulation and experiment, we presented the measured results for the APS-U rf-gaskets and BPM-bellows assembly, and gave a brief summary of impedance considerations and measurements for the gate valve liner and pumping cross. The measured results showed that the APS-U BPM-bellows assembly, gate valve liner, and the pumping cross have been properly designed and manufactured to specifications, with no observable resonance peaks. On the other hand, impedance evaluations of several flange designs have displayed resonances that we subsequently attributed to improper machining and/or poor tolerance control, and we have worked to ensure future designs can be made to specifications. Finally, we showed that the G-line is a relatively simple tool to measure vacuum component impedance over a broad frequency range.

ACKNOWLEDGMENTS

The authors would like to thank X. Sun for CST help, B. Stillwell and J. Carter for providing the .stl simulation files and for ordering the measurement and test equipment,

A. Brill for TDR measurement help, and H. Cease for providing important guidance and support throughout this work. Mr. Sangroula is very thankful to his advisor Prof. Carlo Segre at Illinois Institute of Technology for providing this research opportunity, and invaluable mentoring during his Ph.D. program. This work was supported by the U.S. Department of Energy, Office of Science by Argonne National Laboratory under Contract No. DE-AC02-06CH11357.

[1] M. Borland, Ultra-low-emittance light sources, Synchrotron Radiat. News **27**, 2 (2014).

[2] R. Hettel, Dlsr design and plans: an international overview, J. Synchrotron Radiat. **21**, 843 (2014).

[3] M. Eriksson, J. F. van der Veen, and C. Quitmann, Diffraction-limited storage rings–a window to the science of tomorrow, J. Synchrotron Radiat. **21**, 837 (2014).

[4] A. W. Chao, *Physics of Collective Beam Instabilities in High-Energy Accelerators* (Wiley, New York, 1993).

[5] V. Smaluk, Impedance computations and beam-based measurements: A problem of discrepancy, Nucl. Instrum. Methods Phys. Res., Sect. A **888**, 22 (2018).

[6] A. Faltens, E. C. Hartvig, D. Mohl, and A. M. Sessler, An analog method for measuring the longitudinal coupling impedance of a relativistic particle beam with its environment, Technical report, Lawrence Berkeley National Lab. (LBNL), Berkeley, CA (United States), 1971.

[7] M. Sands and J. Rees, Slac-Report No. pep-95, 1974.

[8] H. Hahn and F. Pedersen, *Coaxial Wire Measurements of the Longitudinal Coupling Impedance (No. BNL-50870)* (Brookhaven National Lab., Upton, NY, 1978), https://www.osti.gov/servlets/purl/6591101.

[9] L. S. Walling, D. E. McMurry, D. V. Neuffer, and H. A Thiessen, Transmission-line impedance measurements for an advanced hadron facility, Nucl. Instrum. Methods Phys. Res., Sect. A **281**, 433 (1989).

[10] U. Niedermayer, L. Eidam, and O. Boine-Frankenheim, Analytic modeling, simulation and interpretation of broadband beam coupling impedance bench measurements, Nucl. Instrum. Methods Phys. Res., Sect. A **776**, 129 (2015).

[11] F. Caspers, Impedance determination from bench measurements, CERN Technical Report No. CERN-PS-2000-004-RF, 2000, https://cds.cern.ch/record/437306/files/ps-2000-004.pdf.

[12] G. R. Lambertson, A. F. Jacob, R. A. Rimmer, and F. Voelker, Techniques for beam impedance measurements above cutoff, Technical report, Lawrence Berkeley Lab., 1990.

[13] M. Sangroula, R. Lill, R. Lindberg, and X. Sun, Impedance measurement of vacuum chamber components for the advance photon source (aps) upgrade, in *8th Int. Particle Accelerator Conf.(IPAC'17), Copenhagen, Denmark, 14-19 May, 2017* (JACOW, Geneva, Switzerland, 2017), pp. 3583–3586, https://accelconf.web.cern.ch/ipac2017/papers/wepva134.pdf.

[14] J. Musson, K. Cole, and S. Rubin, Application of Goubau surface wave transmission line for improved bench testing of diagnostic beamline elements, Technical report, Thomas Jefferson National Accelerator Facility, Newport News, VA (United States), 2009, https://accelconf.web.cern.ch/pac2009/papers/th6rep047.pdf.

[15] F. Stulle and J. Bergoz, Surface waves for testing of beam instrumentation, in *Proceedings of the 3rd International Particle Accelerator Conference, New Orleans, LA, 2012* (IEEE, Piscataway, NJ, 2012), p. 10, https://pdfs.semanticscholar.org/0473/c7cde5574ea1c5ddf53b22b6cce-5246a2709.pdf?_ga=2.199789933.234981343.1597091577-835814721.1596201448.

[16] G. Goubau, Surface waves and their application to transmission lines, J. Appl. Phys. **21**, 1128 (1950).

[17] F. Stulle, J. Musson, and J. Bergoz, Goubau line beam instrumentation testing, the benefits, Proc. IPAC 2014 (2014), https://accelconf.web.cern.ch/IPAC2014/papers/thpme096.pdf.

[18] F. Stulle, J. Bergoz, and H. W. Glock, Measurement of coupling impedances using a Goubau line, in *Proceedings of 5th Int. Beam Instrumentation Conf.(IBIC'16), Barcelona, Spain, Sept. 13-18, 2016* (JACOW, Geneva, Switzerland, 2017), pp. 720–723, https://accelconf.web.cern.ch/ibic2016/papers/wepg41.pdf.

[19] S. Y. Kim, F. Stulle, C. K. Sung, K. H. Yoo, J. Seok, K. J. Moon, C. U. Choi, Y. Chung, G. Kim, H. J. Woo *et al.*, Characterization of the Goubau line for testing beam diagnostic instruments, J. Instrum. **12**, P12016 (2017).

[20] A. Sommerfeld, Über die fortpflanzung elektrodynamischer wellen längs eines drahtes, Ann. der Physik und Chemie **67**, 233 (1899).

[21] J. Zenneck, Über die fortpflanzung ebener elektromagnetischer wellen längs einer ebenen leiterfläche und ihre beziehung zur drahtlosen telegraphie, Ann. Phys. (Berlin) **328**, 846 (1907).

[22] G. Goubau, Single-conductor surface-wave transmission lines, Proceedings of the IRE **39**, 619 (1951).

[23] F. Harms, Elektromagnetische wellen an einem draht mit isolierender zylindrischer hülle, Ann. Phys. (Berlin) **328**, 44 (1907).

[24] J. Stratton, *Electromagnetic Theory* (John Wiley & Sons, New York, 2007).

[25] M. Sangroula, R. Lindberg, R. Lill, and R. Zabel, Measuring the coupling impedance of vacuum components for the APS upgrade using a Goubau line, in *9th Int. Particle Accelerator Conf.(IPAC'18), Vancouver, Canada, 29 Apr—4 May, 2018* (JACOW, Geneva, Switzerland, 2018), pp. 3211–3214, http://accelconf.web.cern.ch/ipac2018/papers/thpak005.pdf.

[26] M. Spata, T. L. Allison, K. E. Cole, J. Musson, and J. Yan, Evaluation and correction of the non-linear distortion of cebaf beam position monitors, Technical report, Thomas Jefferson National Accelerator Facility, Newport News, VA (United States), 2011.

[27] G. Goubau, Surface wave transmission line, US Patent 2,685,068 A, July 27 1954.

[28] R. W. Klopfenstein, A transmission line taper of improved design, Proceedings of the IRE **44**, 31 (1956).

[29] R. P. Hecken, A near-optimum matching section without discontinuities, IEEE Trans. Microwave Theory Techn. **20**, 734 (1972).

[30] J. A. Strickland, H. A. Zimmerman, G. Long, and G. Frye, *Time-Domain Reflectometry Measurements, Measurement Concepts*, 1st ed. (tektronix. Inc., Beaverton, Oregon, USA, 1970).

[31] R. Lindberg *et al.*, Advanced photon source upgrade project preliminary design report, Technical Report No. APSU-2.01-RPT-002, Argonne National Lab, September 2017, https://www.aps.anl.gov/APS-Upgrade/Documents.

[32] V. G. Vaccaro, Coupling impedance measurements, Technical Report No. SCAN-9502087, 1994.

[33] E. Jensen, An improved log-formula for homogeneously distributed impedance, Report No. CERN-PS-RF-NOTE-2000-001, 2000, https://cds.cern.ch/record/960162/files/cer-002626446.pdf.

[34] H. Hahn, Validity of coupling impedance bench measurements, Phys Rev. Accel. Beams **3**, 122001 (2000).

[35] M. P. Sangroula, Coupling impedance measurement and analysis of critical vacuum chamber components for the Advanced Photon Source Upgrade, Ph.D. thesis, Illinois Institute of Technology, 2018.